Journal of Zhejiang University-SCIENCE C (Computers & Electronics)
ISSN 1869-1951 (Print); ISSN 1869-196X (Online)
www.zju.edu.cn/jzus; www.springerlink.com
E-mail: jzus@zju.edu.cn

Extracting DC bus current information for optimal phase correction and current ripple in sensorless brushless DC motor drive*

Zu-sheng HO, Chii-maw UANG†‡, Ping-chieh WANG
(*Department of Electronic Engineering, I-Shou University, Taiwan 84001, Kaohsiung*)
†E-mail: ucmk@isu.edu.tw

Received Sept. 6, 2013; Revision accepted Jan. 15, 2014; Crosschecked Mar. 17, 2014

Abstract: Brushless DC motor (BLDCM) sensorless driving technology is becoming increasingly established. However, optimal phase correction still relies on complex calculations or algorithms. In finding the correct commutation point, the problem of phase lag is introduced. In this paper, we extract DC bus current information for auto-calibrating the phase shift to obtain the correct commutation point and optimize the control of BLDC sensorless driving. As we capture only DC bus current information, the original shunt resistor is used in the BLDCM driver and there is no need to add further current sensor components. Software processing using only simple arithmetic operations successfully accomplishes the phase correction. Experimental results show that the proposed method can operate accurately and stably at low or high speed, with light or heavy load, and is suitable for practical applications. This approach will not increase cost but will achieve the best performance/cost ratio and meet market expectations.

Key words: Brushless motors, Electric motors, Motor drives, Phase control, Phase estimation, Sensorless control
doi:10.1631/jzus.C1300247 **Document code:** A **CLC number:** TM301.2

1 Introduction

Recently, energy saving and carbon reduction issues have become part of everyday life. Brushless DC motors (BLDCMs) have a simple structure and miniaturization characteristics, and the rapid progress of power electronics technology has greatly improved their reliability and reduced maintenance costs, creating the potential of limitless future development. Structured with permanent magnets, the efficiency of BLDCMs is higher than that of traditional motors (Gambetta and Ahfock, 2009). However, they require a sensor to detect the rotor position for proper commutation. In general, hall sensors are used for reporting the rotor position information, but the hall sensor cannot perform well in any high temperature or noisy environment. To overcome this limitation, engineers have focused on sensorless drive technology (Acarnley and Watson, 2006; Chen and Cheng, 2006; Chen *et al*., 2007; Abolfazl *et al*., 2009; Chen *et al*., 2009). Detecting the direct back electro-motive force (BEMF) is one of the most widely used methods for obtaining the rotor position information. The pulse-width modulation (PWM) signals switch the metal–oxide–semiconductor field-effect transistor (MOSFET) to adjust the speed of the BLDCM; thus, the noise induced from PWM signals remains in the phase voltage. To extract the BEMF, a low-pass filter is generally used to filter out the noise of the phase voltage. Going through the filter circuit, the phase angle information of the voltage will be shifted and also, the zero crossing point (rotor position signal) lags. To overcome this problem, the lookup table method is often used to perform the phase compensation (Kim and Ehsani, 2003; Shen and Tseng, 2003).

‡ Corresponding author
* Project supported by the I-Shou University (No. ISU99-01-04), the Holtek Semiconductor Inc. (No. ISU99-e-02), and the DurQ Machinery Corp. (No. ISU101-IND-13)
© Zhejiang University and Springer-Verlag Berlin Heidelberg 2014

As the lag amount depends on the running speed, the method needs to record the shifted angle prior to detecting the sensorless rotor position signal. Most sensorless BLDC motors are without any space for placing the hall sensor; thus, prior recording of the lag offset is very difficult. Obviously, the lookup table method is simple but recording the lag offset requires too much time to create the compensation table, and the accuracy of the lagging information obtained is unreliable.

A previous technology uses the non-conduction phase of the freewheeling current characteristic to achieve real-time phase correction. Although this method can perform phase correction, it cannot compensate correctly for the phase delay caused by high running speeds (Uang *et al*., 2011). Also, note that PWM in 100% duty does not have PWM switching characteristics and the freewheeling current effect will be undetectable during the unexcited phase. Although the phase shift is very serious, driving in very heavy load conditions causes the large current to occur in the unexcited phase period; thus, the PWM in 100% duty will lose its accuracy. Moreover, reducing torque ripple by using the unexcited phase period of the freewheeling current technique cannot work either, because the unexcited phase freewheeling current does not exist. In terms of hardware cost, monitoring only the DC bus current requires only one current sensor, whereas monitoring three phases needs three current sensors.

Whether sensor or sensorless driven, another headache for driving BLDCMs is that the compensated angle is fixed and cannot vary according to the running state (speed or loading). We know that the BEMF voltage and excited current fit well in low speed operation, but not well in other cases. The output torque is stable and the torque ripple is generated only at the commutation point. Owing to an inductive load, as the motor speeds up, the coil inductance effects are more obvious and the excited current increases to affect the BEMF phase lagging. Clearly, when the exciting current is saturated, the motor cannot generate any more output torque. This will result in phase lagging. In this condition, sharp current waves exist in the rear part of phase current, which causes the current ripple to generate vibration and noise, posing a threat to the power components. The greater the current spike, the greater the difference between the average current and the root mean square (RMS) current, and the greater the winding losses, leading to a reduction in output efficiency. Therefore, the electromagnetic time constant, which presents nonlinear characteristics, should not be ignored during high speed operations (Chuang *et al*., 2009; Salah *et al*., 2011; Han and Zhang, 2012). It is very clear that a stable drive system must reduce the current ripple as much as possible, or it will not perform well in high efficiency brushless motor driving.

The proposed method detects only the system current to achieve real-time phase compensation for the BLDCM sensorless drive. Auto-calibration improves the phase lagging commutation caused by the low-pass filter and also optimizes torque ripple caused by the motor inductance characteristics when running at a high speed. Note that compared with the freewheeling current of the unexcited phase method, here the cost of the current sensors can be saved. Considering software cost, the method uses only a simple arithmetic operation to complete the correct commutation task and to maintain the phase correction, which ensures that the system current is undistorted and smooth and achieves minimum torque ripple. The torque ripple problem has been discussed in direct torque control (Liu *et al*., 2005), improvements of PWM techniques, motor model compensation, and current control for reduced torque ripple (Dixon and Leal, 2002; Salah *et al.*, 2011). We want to emphasize that the proposed method is primarily intended to use the information hidden inside the DC bus current trace to solve the phase shift problem of BLDCM sensorless driving and that improvements in the torque ripple are additional benefits. Therefore, the proposed method should not be compared with those techniques specifically aimed at reducing electrical commutation current characteristics of the BLDC method.

2 Electrical commutation current characteristics of BLDCM

A three-phase star connected winding BLDCM is shown in Fig. 1, in which AT, BT, and CT are MOSFET of the top arm, and AB, BB, and CB are the MOSFET of the bottom arm. By this configuration, three stator phase voltages can be written as

$$\begin{cases} u_{\mathrm{a}} = Ri_{\mathrm{a}} + e_{\mathrm{a}}(\xi) + L_{\sigma}\dfrac{\mathrm{d}i_{\mathrm{a}}}{\mathrm{d}t} + u_{\mathrm{n}}, \\ u_{\mathrm{b}} = Ri_{\mathrm{b}} + e_{\mathrm{b}}(\xi) + L_{\sigma}\dfrac{\mathrm{d}i_{\mathrm{b}}}{\mathrm{d}t} + u_{\mathrm{n}}, \\ u_{\mathrm{c}} = Ri_{\mathrm{c}} + e_{\mathrm{c}}(\xi) + L_{\sigma}\dfrac{\mathrm{d}i_{\mathrm{c}}}{\mathrm{d}t} + u_{\mathrm{n}}, \\ i_{\mathrm{a}} + i_{\mathrm{b}} + i_{\mathrm{c}} = 0, \end{cases} \tag{1}$$

where u_{a}, u_{b}, and u_{c} are phase voltages of the stator, R is the phase resistance, L_{σ} is the phase inductance, i_{a}, i_{b}, and i_{c} are the phase currents, u_{n} is the neutral voltage, e_{a}, e_{b}, and e_{c} are the BEMF of each phase, and ξ is the electrical angle.

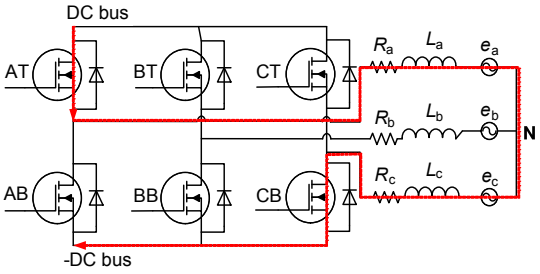

Fig. 1 Conducting stage of phase-A and phase-C

The three-phase BLDCM is driven using a six-step commutation strategy, also known as two-phase conducting or 120° commutation. This means that during each electrical cycle of 360°, there are two 60° states for high voltage, two 60° states for low voltage, and two other 60° non-conducting states. We take the conducting stages of phase-A and phase-C changing to phase-B and phase-C as an example to analyze the BLDCM operation equations.

The commutation process can be divided into three stages: (1) Before the commutation point, the current flows through phase-A to phase-C (Fig. 1); (2) Right at the commutation point, the current switches from phase-A and phase-C to phase-B and phase-C (Fig. 2); (3) After the commutation point, the current flows through phase-B to phase-C (Fig. 3).

At the switching point, when the conducting stage of phase-A and phase-C changes to phase-B and phase-C, the AT is switched off and BT is switched on to the DC bus (U). The conducting current is $i_{\mathrm{a}}=-i_{\mathrm{c}}=i_{\mathrm{s}}$. From the equivalent circuit diagram shown in Fig. 2, the following equation can be derived:

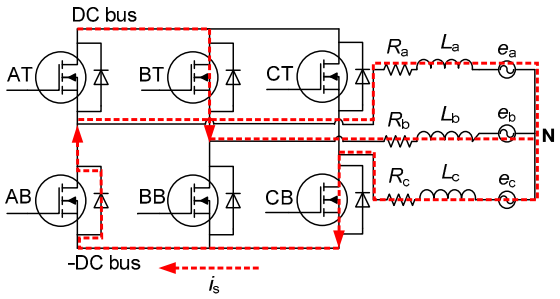

Fig. 2 The commutation point where current switches from phase-A and phase-C to phase-B and phase-C

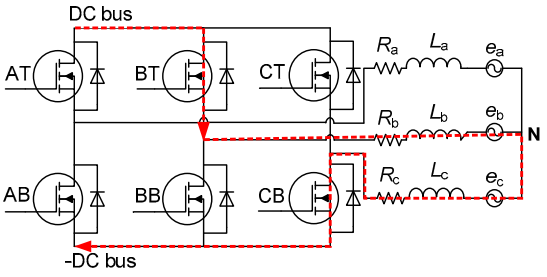

Fig. 3 Conducting stage of phase-B and phase-C

$$\begin{cases} Ri_{\mathrm{a}} + L_{\sigma}\dfrac{\mathrm{d}i_{\mathrm{a}}}{\mathrm{d}t} + e_{\mathrm{a}}(\xi) - e_{\mathrm{c}}(\xi) - L_{\sigma}\dfrac{\mathrm{d}i_{\mathrm{c}}}{\mathrm{d}t} - Ri_{\mathrm{c}} = 0, \\ Ri_{\mathrm{b}} + L_{\sigma}\dfrac{\mathrm{d}i_{\mathrm{b}}}{\mathrm{d}t} + e_{\mathrm{a}}(\xi) - e_{\mathrm{c}}(\xi) - L_{\sigma}\dfrac{\mathrm{d}i_{\mathrm{c}}}{\mathrm{d}t} - Ri_{\mathrm{c}} = U, \\ i_{\mathrm{a}} + i_{\mathrm{b}} + i_{\mathrm{c}} = 0, \\ i_{\mathrm{a}} = i_{\mathrm{s}},\ i_{\mathrm{b}} = 0,\ i_{\mathrm{c}} = -i_{\mathrm{s}}. \end{cases} \tag{2}$$

Let $\tau=L_{\sigma}/R$ be the electromagnetic time constant and E the BEMF voltage. Adding τ to Eq. (2), we have

$$\begin{cases} i_{\mathrm{a}}(t) = -\dfrac{U+2E}{3R} + \left(i_{\mathrm{s}} + \dfrac{U+2E}{3R}\right)\mathrm{e}^{-t/\tau}, \\ i_{\mathrm{b}}(t) = \dfrac{2U-2E}{3R} + \dfrac{2E-2U}{3R}\mathrm{e}^{-t/\tau}, \\ i_{\mathrm{c}}(t) = \dfrac{4E-U}{3R} - \left(i_{\mathrm{s}} + \dfrac{4E-U}{3R}\right)\mathrm{e}^{-t/\tau}. \end{cases} \tag{3}$$

When $t=t_{\mathrm{a}}$, phase-A current drops to zero and then at the end of commutation, $i_{\mathrm{a}}(t_{\mathrm{a}})=0$. The motor will go to the conducting stage of phase-B and phase-C, and the current is an initial value of phase-B and phase-C. By $i_{\mathrm{a}}(t_{\mathrm{a}})=0$ we can obtain

$$t_{\mathrm{a}} = -\tau \ln\left(\frac{U+2E}{3Ri_{\mathrm{s}}+U+2E}\right). \tag{4}$$

At the end of commutation, the phase-B and phase-C current can be derived:

$$\begin{cases} i_{\mathrm{b}}(t_{\mathrm{a}}) = \dfrac{(2U-2E)i_{\mathrm{s}}}{3Ri_{\mathrm{s}}+U+2E}, \\ i_{\mathrm{c}}(t_{\mathrm{a}}) = -\dfrac{(2U-2E)i_{\mathrm{s}}}{3Ri_{\mathrm{s}}+U+2E}. \end{cases} \tag{5}$$

From the equivalent circuit diagram shown in Fig. 3, the phase-B and phase-C conducting equation can be derived:

$$\begin{cases} Ri_{\mathrm{b}} + L_\sigma \dfrac{\mathrm{d}i_{\mathrm{b}}}{\mathrm{d}t} + e_{\mathrm{a}}(\xi) - e_{\mathrm{c}}(\xi) - L_\sigma \dfrac{\mathrm{d}i_{\mathrm{c}}}{\mathrm{d}t} - Ri_{\mathrm{c}} = U, \\ i_{\mathrm{b}} = -i_{\mathrm{c}}, \\ i_{\mathrm{b}}(0+) = \dfrac{(2U-2E)i_{\mathrm{s}}}{3Ri_{\mathrm{s}}+U+2E}, \\ i_{\mathrm{c}}(0+) = -\dfrac{(2U-2E)i_{\mathrm{s}}}{3Ri_{\mathrm{s}}+U+2E}. \end{cases} \tag{6}$$

From Eq. (6), the phase-B and phase-C conducting current can be derived:

$$\begin{cases} i_{\mathrm{b}}(t) = \dfrac{U-2E}{2R} + \dfrac{(U+2E)(Ri_{\mathrm{s}}-U+2E)}{2R(3Ri_{\mathrm{s}}+U+2E)}\mathrm{e}^{t/\tau}, \\ i_{\mathrm{c}}(t) = -\dfrac{U-2E}{2R} - \dfrac{(U+2E)(Ri_{\mathrm{s}}-U+2E)}{2R(3Ri_{\mathrm{s}}+U+2E)}\mathrm{e}^{-t/\tau}. \end{cases} \tag{7}$$

In a symmetrical three-phase system, the phase-B winding current, according to Eqs. (5) and (7), can be deduced for each electric cycle, as shown in Eq. (8). In Eq. (8), t_1 is the phase current that drops to zero at t_{a}; t_2=10/(Pn); t_3=t_2+t_{a}; t_4=20/(Pn); t_5=t_4+t_{a}; t_6=30/(Pn); t_7=t_6+t_{a}; t_8=40/(Pn); t_9=t_8+t_{a}; t_{10}=50/(Pn); t_{11}=t_{10}+t_{a}; t_{12}=60/(Pn). P is the number of poles, and n is the rotating speed (r/min).

Eq. (8) is the ideal current waveform whose ideal phase current waveform can be depicted as shown in Fig. 4. From Eq. (8) and Fig. 4 we can clearly observe the current flowing through the winding. Obviously, during the upper-bridge conducting period, interval t_1–t_2 is identical to t_3–t_4; during the lower-bridge conducting period, interval t_7–t_8 is identical to t_9–t_{10}. This exhibits the symmetrical mapping relationship between the upper-bridge and lower-bridge.

$$\begin{cases} \dfrac{2U-2E}{3R} + \dfrac{2E-2U}{3R}\mathrm{e}^{\frac{t}{\tau}}, & 0 \le t \le t_1, \\ \dfrac{U-2E}{2R} + \dfrac{(U+2E)(Ri_{\mathrm{s}}-U+2E)}{2R(3Ri_{\mathrm{s}}+U+2E)}\mathrm{e}^{\frac{t-t_1}{\tau}}, & t_1 \le t \le t_2, \\ \dfrac{U-4E}{3R} + \left(i_{\mathrm{s}} + \dfrac{4E-U}{3R}\right)\mathrm{e}^{\frac{t-t_2}{\tau}}, & t_2 \le t \le t_3, \\ \dfrac{U-2E}{2R} + \dfrac{(U+2E)(Ri_{\mathrm{s}}-U+2E)}{2R(3Ri_{\mathrm{s}}+U+2E)}\mathrm{e}^{\frac{t-t_3}{\tau}}, & t_3 \le t \le t_4, \\ -\dfrac{U+2E}{3R} + \left(i_{\mathrm{s}} + \dfrac{U+2E}{3R}\right)\mathrm{e}^{\frac{t-t_4}{\tau}}, & t_4 \le t \le t_5, \\ 0, & t_5 \le t \le t_6, \\ -\dfrac{2U-2E}{3R} - \dfrac{2E-2U}{3R}\mathrm{e}^{\frac{t-t_6}{\tau}}, & t_6 \le t \le t_7, \\ -\dfrac{U-2E}{2R} - \dfrac{(U+2E)(Ri_{\mathrm{s}}-U+2E)}{2R(3Ri_{\mathrm{s}}+U+2E)}\mathrm{e}^{\frac{t-t_7}{\tau}}, & t_7 \le t \le t_8, \\ -\dfrac{U-4E}{3R} - \left(i_{\mathrm{s}} + \dfrac{4E-U}{3R}\right)\mathrm{e}^{\frac{t-t_8}{\tau}}, & t_8 \le t \le t_9, \\ -\dfrac{U-2E}{2R} - \dfrac{(U+2E)(Ri_{\mathrm{s}}-U+2E)}{2R(3Ri_{\mathrm{s}}+U+2E)}\mathrm{e}^{\frac{t-t_9}{\tau}}, & t_9 \le t \le t_{10}, \\ \dfrac{U+2E}{3R} - \left(i_{\mathrm{s}} + \dfrac{U+2E}{3R}\right)\mathrm{e}^{\frac{t-t_{10}}{\tau}}, & t_{10} \le t \le t_{11}, \\ 0, & t_{11} \le t \le t_{12}. \end{cases} \tag{8}$$

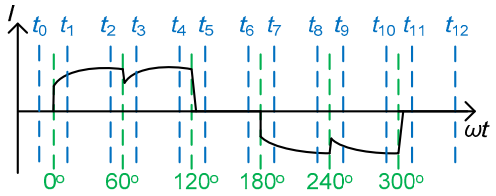

Fig. 4 Ideal waveform of phase current

The current waveforms of the DC bus, phase-A, phase-B, and phase-C are shown in Fig. 5. As the total current of the DC bus generates the motor torque, the torque is the output power divided by the mechanical angle:

$$T_{\mathrm{e}} = P_{\mathrm{out}} / \omega_{\mathrm{m}}, \tag{9}$$

where T_{e} is the torque, P_{out} is the output power, and ω_{m} is the mechanical speed.

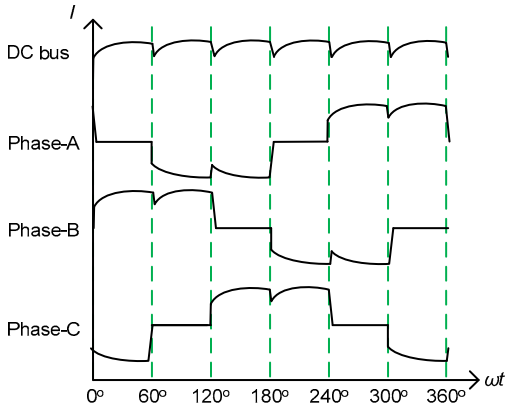

Fig. 5 BLDCM three-phase currents and DC bus current

As the three-phase BLDCM output power is $(e_a i_a+e_b i_b+e_c i_c)/\omega_m$, the T_e torque equation can be written as follows:

$$T_e = \frac{e_a i_a + e_b i_b + e_c i_c}{\omega_m}. \tag{10}$$

Let $e_n=K_e\omega_m$ (n=a, b, c). We obtain

$$T_e = K_e(i_a + i_b + i_c), \tag{11}$$

where K_e is the back-EMF constant.

According to Eqs. (9) and (11), we can find that P_{out} is proportional to i_a, i_b, and i_c, prove that the torque ripple is proportional to the winding current, and also explain that the missed optimal commutation timing is equivalent to the contribution of phase leading or lagging status. Thus, either the rotor position signal going through low pass filter or the motor running at high speed will result in phase lagging. However, the phase angle being over compensated will result in a phase leading. In both cases, the DC bus current will be disturbed. We need only to carefully control and adjust the DC bus current to work smoothly. The minimized current ripple will be easily achieved.

3 Extracting phase shift information from DC bus current

As described earlier, bus current is a direct reflection of the three-phase current information. The system diagram for real-time phase shift correction is depicted in Fig. 6a and the actual hardware setup is shown in Fig. 6b. The system power provides the DC bus voltage driving the BLDCM. The DC-DC converter has three DC voltage outputs: DC15 V for the gate driver and 5 V and 3.3 V for the microprocessor system. A sensorless circuit is based on comparing phase-to-phase BEMF voltage to detect the zero crossing point and obtain the rotor position signals in Ho *et al*. (2013). The system current is extracted from a differential amplifier voltage which is obtained by a shunt resistor, and the system current is used to correct the shifted angle. The entire task is executed by a low cost MCU, HOLTEK-32-bit ARM Cortex-M3. Fig. 6b is the hardware setup of the system block diagram, which is the whole hardware experimental platform. In the load test, DC electronic load by the generator is used via rectifier circuit, which converts the three-phase AC voltage to DC voltage, and an oscilloscope is used to record the experimental results.

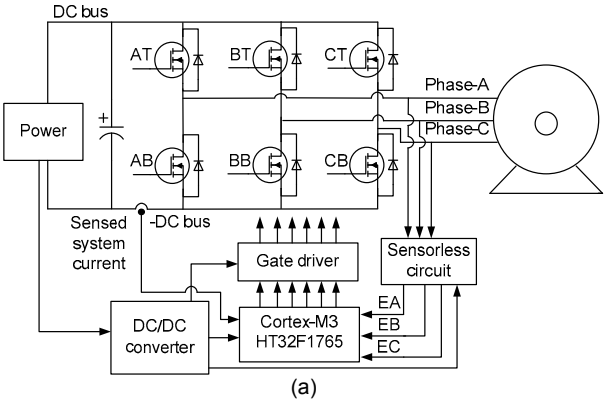

(a)

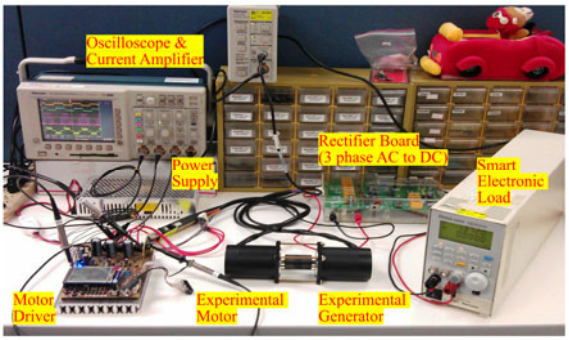

(b)

Fig. 6 System architecture for the system block diagram (a) and the experimental platform (b)

We take phase-B as an example to explain how to extract the phase shift information from the system DC bus current. A typical DC bus current waveform

and phase-B conducting current are shown in Fig. 7. For ease of comprehension, we divide the 0–60° in the phase-B upper bridge conducting period into two regions of 0–30° named ① and 30°–60° named ②. In these two regions, the phase current varies with the load, no load, or high speed condition, because of the BLDCM inductance characteristics. However, they do have a similar path and span, as shown by the horizontal dashed lines in Fig. 7. According to our experience and observation, it is found that the phase shift information can be obtained by comparing the change in the span of the current curve in the intervals of regions ① and ②.

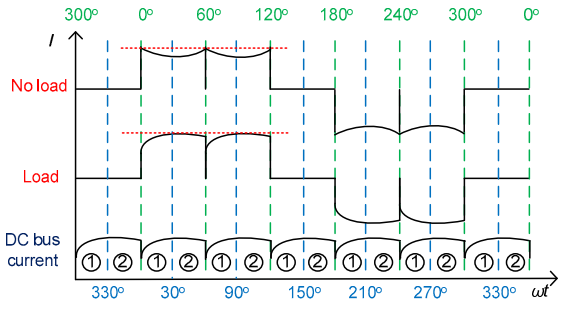

Fig. 7 Ideal current waveform of phase-B and DC bus current extraction steps within one electric cycle

To compare the changing trend of the current curve, a systematic procedure is described in the following. In accordance with the way in which the hall sensor represents the rotor position, in our system a three-bit commutation signal named EA, EB, and EC is established, where EC is the most significant bit (MSB) and EA the least significant bit (LSB). The relationship between the electrical degree and switching sequence is fixed and the retrieved current value must be stored in the corresponding registers. The driving of a three-phase BLDCM by 120° trapezoidal wave commutation implies that the upper arm of the MOSFET is on 120° but for each 60°, it is changed to turn on the lower arm of the MOSFET of the inverter. Whenever the commutation signal changes, the flag is reset to 0 and the current DC bus current maximum value is recorded in REG1. After 30°, the flag is set to 1 and the maximum value of the DC bus current is recorded in REG2. To clarify the sequence of captured DC bus values and storage locations within an electrical cycle, we list them in Table 1 for easy reference.

Table 1 The sequence of captured DC bus values and storage locations within an electrical cycle

Phase range (°)	(CS) EC EB EA	Flag	ON MOSFETs	Extracted information*
0–30	(5) 1 0 1	0	BT CB	REG1
30–60	(5) 1 0 1	1	BT CB	REG2
60–90	(4) 1 0 0	0	AT CB	REG1
90–120	(4) 1 0 0	1	AT CB	REG2
120–150	(6) 1 1 0	0	AT BB	REG1
150–180	(6) 1 1 0	1	AT BB	REG2
180–210	(2) 0 1 0	0	CT BB	REG1
210–240	(2) 0 1 0	1	CT BB	REG2
240–270	(3) 0 1 1	0	CT AB	REG1
270–300	(3) 0 1 1	1	CT AB	REG2
300–330	(1) 0 0 1	0	BT AB	REG1
330–0	(1) 0 0 1	1	BT AB	REG2

CS: commutation signal. Three-bit commutation signal named EA, EB, and EC is established, where EC is the MSB and EA the LSB.
* The REG in which the maximum system current value captured is recorded

The algorithms of auto-phase correction can be divided into two parts:

1. Extraction of the DC bus current information

Fig. 7 shows the DC bus current processing process in one electric cycle. It includes six steps and each step can be further divided into two regions (① and ②) for discussion.

In region ①:

Step 1: Detect the occurrence of a commutation signal change.

Step 2: Wait until the optimized phase commutation signal is obtained.

Step 3: Do commutation.

Step 4: Move previous maximum current information (in REG1 and REG2) to temporary registers (REG1_TEMP and REG2_TEMP).

Step 5: Reset flag to 0.

Step 6: Obtain the first new maximum current information recorded in REG1.

In region ②:

Step 1: Wait until a 30° rotation of correct commutation.

Step 2: Set flag to 1.

Step 3: Obtain the second new maximum current information recorded in REG2.

Step 4: Call the 'phase corrector' to do phase correction.

2. Phase processing and optimization

REG1_TEMP and REG2_TEMP save the previous maximum DC bus current of regions ① and ②, respectively. A flowchart of auto-phase correction called the 'phase corrector' is depicted in Fig. 8. At the end of region ② (before the start of the next region ①) the phase corrector will be called to find the shifted angle using the values of REG1_TEMP and REG2_TEMP. If REG1_TEMP is smaller than REG2_TEMP, the status of the commutation signal is phase lagging; otherwise, the status is phase leading. A synchronous phase is found when the result is neither of these two cases. If any leading or lagging status is found, the next commutation point will be corrected by phase compensation. The shifted angle is continuously corrected until a synchronous status is found. It is clear that the operations used in the phase corrector compare only the values of REG1_TEMP and REG2_TEMP, which is a simple arithmetic operation.

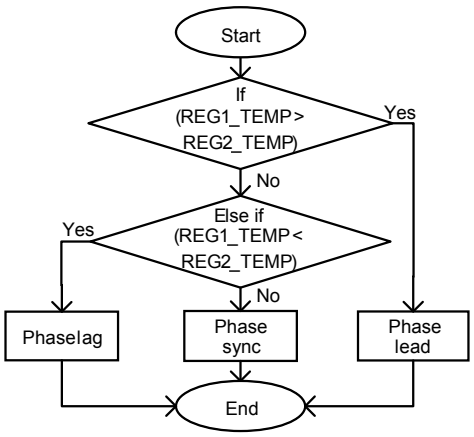

Fig. 8 Flowchart of the phase corrector

It can be seen that the phase corrector will correct the phase angle dynamically by detecting the DC bus status. After obtaining the phase shift information, the minimum torque ripple can be determined easily. To implement the phase corrector, we need only an A/D convertor and two general purpose timers. In a real application, most low cost MCUs can perform these tasks well. In this way, the use of simple and low cost MCUs can optimize the best performance of sensorless driving.

4 Experimental results

Experiments were conducted to verify and compare the proposed method with that in Uang *et al*. (2011). From Uang *et al*. (2011), it is clear that when commutation is done at the correct phase point, the two freewheeling currents of the unexcited phase are equal during each full electric cycle. However, due to the impact of the winding inductance characteristic, a large torque ripple will be induced at high speeds, although in the correct commutation phase. The induced large torque will reduce the efficiency and generate noise and vibration. Note that the freewheeling current characteristics cannot be clearly caught when the PWM is set nearly at the full duty cycle (duty over 98%). To observe the freewheeling current conducting phenomenon of the PWM switched between low and high speed situations, we set the PWM duty at 30% and 100%, giving the same load, to compare their differences. The waveforms were recorded using an oscilloscope (Figs. 9–12). In the following figures, channel 1 is colored yellow and denotes the phase-B phase current, channel 2 is colored blue and denotes the sensorless commutation signal, channel 3 is colored pink and denotes the phase-B voltage, and channel 4 is colored green and denotes the DC bus current (References to color refer to the online version of this paper). A general purpose BLDCM with 10 poles, rated power 80 W, rated voltage 24 V, rated torque 2.6 kg·cm, winding resistance 210 mΩ, winding inductor 300 μH, and rotating speed 3000 r/min was used as the experimental target.

We compared the freewheeling current characteristic in 30% and 100% PWM duty conditions. For clarity, the scale of the phase current has been magnified. In Fig. 9, the unexcited phase method was applied, as presented in Uang *et al*. (2011). We can see that the two freewheeling currents of the two unexcited phases were equal during each full electric cycle. The running speed was 1626 r/min and the DC bus current ripple was 1.8 A. In Fig. 10, the proposed

method was applied. We can see that the two freewheeling currents of the two unexcited phases were not equal during each full electric cycle, because the phase angle was automatically advanced to force the system current flat-topped waveform by calling the phase corrector. However, the running speed was 1646 r/min, increased by 20 r/min, and the DC bus current ripple was 1.2 A, reduced by 33%. These greatly improved results can be explained as follows: in the 100% duty condition, there is no PWM switching signal; thus, the unexcited phase freewheeling current will not exist, and the freewheeling characteristic does not show up. However, our proposed method does not have this problem. Comparing Figs. 11 and 12, the current ripple was reduced by 17% from 1.8 to 1.4 A, and the speed was increased by 18 r/min from 3390 to 3408 r/min. We can see that extracting the DC bus information to correct the phase angle to do phase compensation is a very effective approach. To bolster our argument further, we expanded the experiment and increased PWM duty in 10% increments. The experimental results are summarized in Table 2, including increased running

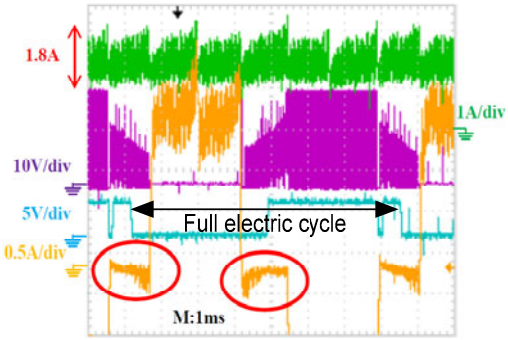

Fig. 9 Results of using the unexcited phase method in the 30% PWM duty condition

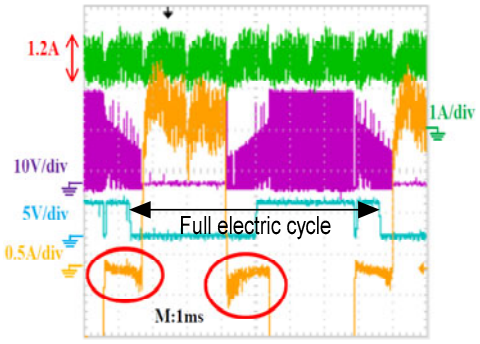

Fig. 10 Results of using the proposed method in the 30% PWM duty condition

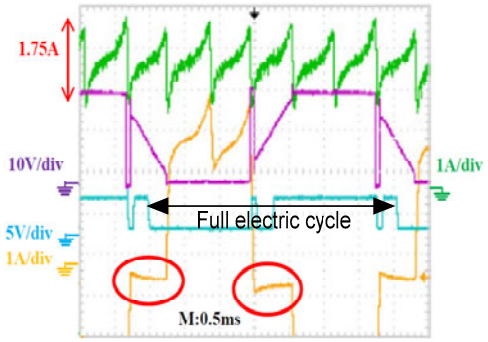

Fig. 11 Results of using the unexcited phase method in the 100% PWM duty condition

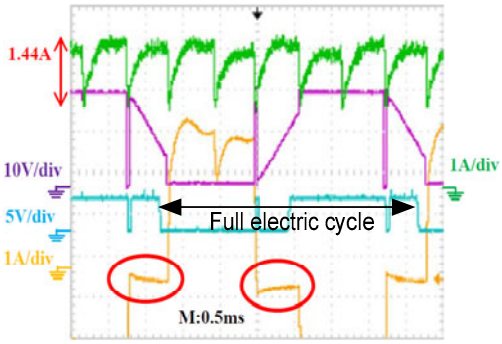

Fig. 12 Results of using the proposed method in the 100% PWM duty condition

Table 2 Comparison of the proposed method and unexcited phase method

PWM duty (%)	Increased speed (r/min)	Reduced current ripple (%)	Advanced degree (°)
10	0	3.3	1.2
20	1.2	12.5	2.0
30	4.8	14.3	3.9
40	9.6	19.1	5.1
50	18.0	18.7	6.1
60	21.6	16.7	7.2
70	31.2	22.9	9.2
80	48.0	17.1	10.5
90	90.0	20.5	11.0
100	118.8	18.8	17.0

speed, reduced current ripple, and advanced degrees. Using our proposed method, the running speed was steadily increased and the current ripple steadily reduced. The increased running speed is the difference between the proposed method and unexcited phase method, which can be obtained from Eq. (12). The percentage of the reduced current ripple can be

obtained using Eq. (13). The phase corrector helps perform the auto-phase advanced, which is the main contributor to the increased speed and reduced current ripple. The advanced degree is calculated using Eq. (14). Obviously, in terms of reduced torque ripple and increased running speed, the proposed method is better than the unexcited phase method in the same PWM duty condition. This is because the proposed method not only performs auto-correction but also reduces torque ripple through phase correction.

$$\mathrm{RPM}_{\mathrm{Inc}} = \mathrm{RPM}_{\mathrm{P}} - \mathrm{RPM}_{\mathrm{U}}, \tag{12}$$

$$\mathrm{I\_ripple}_{\mathrm{Dec}} = \frac{\mathrm{I\_ripple}_{\mathrm{U}} - \mathrm{I\_ripple}_{\mathrm{P}}}{\mathrm{I\_ripple}_{\mathrm{U}}}, \tag{13}$$

$$\mathrm{Adv\_degree} = \mathrm{Degree\_ctrl}_{\mathrm{P}} - \mathrm{Degree\_ctrl}_{\mathrm{U}}, \tag{14}$$

where $\mathrm{RPM}_{\mathrm{Inc}}$ is the increased speed, $\mathrm{RPM}_{\mathrm{P}}$ is the rotation speed of the proposed method, $\mathrm{RPM}_{\mathrm{U}}$ is the rotation speed of the unexcited phase method, $\mathrm{I\_ripple}_{\mathrm{Dec}}$ is the reduced current ripple, $\mathrm{I\_ripple}_{\mathrm{U}}$ is the current ripple of the unexcited phase method, $\mathrm{I\_ripple}_{\mathrm{P}}$ is the current ripple of the proposed method, Adv_degree is the advanced electrical degree, $\mathrm{Degree\_ctrl}_{\mathrm{P}}$ is the control degree of the proposed method, and $\mathrm{Degree\_ctrl}_{\mathrm{U}}$ is the control degree of the unexcited phase method.

5 Conclusions

Experimental results show that the experimental waveform approximated to the theoretical waveform, which proves the correctness of the proposed method. The effectiveness not only auto-calibrates to obtain the correct commutation point but also optimizes the DC bus ripple current induced from winding inductance characteristics when running at a high speed. The proposed method is simple and can be implemented through simple arithmetic operation. Of course, we want to emphasize that this method could be embedded into the hall sensor driver system, which would provide the benefit of reduced torque ripple and overcome the problems of hall sensor misplacement and aging.

References

Abolfazl, H.N., Abolfazl, V., Hassan, M., 2009. Low-cost senseless control of four-switch, brushless DC motor drive with direct back-EMF detection. *J. Zhejiang Univ.-Sci. A*, **10**(2):201-208. [doi:10.1631/jzus.A0820097]

Acarnley, P.P., Watson, J.F., 2006. Review of position sensorless operation of brushless permanent-magnet machines. *IEEE Trans. Ind. Electron.*, **53**(2):352-362. [doi:10.1109/TIE.2006.870868]

Chen, C.H., Cheng, M.Y., 2006. Design of a multispeed winding for a brushless DC motor and its sensorless control. *IET Electr. Power Appl.*, **153**(6):834-841. [doi:10.1049/ip-epa:20060073]

Chen, H.C., Chang, Y.C., Huang, C.K., 2007. Practical sensorless control for inverter-fed BDCM compressors. *IET Electr. Power Appl.*, **1**(1):127-132. [doi:10.1049/iet-epa:20060162]

Chen, H.C., Tsai, T.Y., Huang, C.K., 2009. Low-speed performance comparisons of back-EMF detection circuits with position-dependent load torque. *IET Electr. Power Appl.*, **3**(2):160-169. [doi:10.1049/iet-epa:20080017]

Chuang, H.S., Ke, Y.L., Chuang, Y.C., 2009. Analysis of commutation torque ripple using different PWM modes in BLDC motors. IEEE Industrial Commercial Power System Technical Conf., p.1-6. [doi:10.1109/ICPS.2009.5463966]

Dixon, J.W., Leal, L.A., 2002. Current control strategy for brushless DC motors based on a common DC signal. *IEEE Trans. Power Electron.*, **1**(2):232-240. [doi:10.1109/63.988834]

Gambetta, D., Ahfock, A., 2009. New sensorless commutation technique for brushless DC motors. *IET Electr. Power Appl.*, **3**(1):40-49. [doi:10.1049/iet-epa:20070517]

Han, S.Q., Zhang, Z., 2012. Design of control system for brushless DC motor based on DSP. 2nd Int. Conf. on Materials, Mechatronics and Automation. Lecture Notes in Information Technology, **15**:58-64.

Ho, Z.S., Uang, C.M., Wang, P.C., 2013. Full speed range senesorless circuit for BLDC motor driver. Electronic Technology Symp. Conf., p.519-522.

Kim, T.H., Ehsani, M., 2003. An error analysis of the sensorless position estimation for BLDC motors. IEEE Industry Applications Conf. 38th IAS Annual Meeting, p.611-617. [doi:10.1109/IAS.2003.1257564]

Liu, Y., Zhu, Z.Q., Howe, D., 2005. Direct torque control of brushless DC drives with reduced torque ripple. *IEEE Trans. Ind. Appl.*, **41**(2):599-608. [doi:10.1109/IAS.2004.1348810]

Salah, W.A., Ishak, D., Hammadi, K.J., 2011. Minimization of torque ripples in BLDC motors due to phase commutation—a review. *Przeglad Elektrotechniczny*, **87**:182-188.

Shen, J.X., Tseng, K.J., 2003. Analyses and compensation of rotor position detection error in sensorless PM brushless DC motor drives. *IEEE Trans. Energy Conv.*, **18**(1):87-93. [doi:10.1109/TEC.2002.808339]

Uang, C.M., Ho, Z.S., Wang, P.C., *et al.*, 2011. Sensorless position optimal control strategy of brushless DC motor. IEEE 9th Int. Conf. on Power Electronics and Drive Systems, p.653-658. [doi:10.1109/PEDS.2011.6147321]